

# Fluidization of collisionless plasma turbulence

Romain Meyrand<sup>a,b,1</sup>, Anjor Kanekar<sup>c,d</sup>, William Dorland<sup>c,e</sup>, and Alexander A. Schekochihin<sup>e,f</sup>

<sup>a</sup>LPP, École Polytechnique, F-91128 Palaiseau Cedex, France; <sup>b</sup>Space Sciences Laboratory, University of California, Berkeley, CA 94720, USA; <sup>c</sup>Department of Physics, University of Maryland, College Park, Maryland 20742-3511, USA; <sup>d</sup>Palantir Technologies, 20 Soho Square, London W1D 3QW, UK; <sup>e</sup>Rudolf Peierls Centre for Theoretical Physics, University of Oxford, Clarendon Laboratory, Parks Road, Oxford OX1 3PU, UK; <sup>f</sup>Merton College, Oxford OX1 4JD, UK

This manuscript was compiled on August 14, 2018

In a collisionless, magnetized plasma, particles may stream freely along magnetic-field lines, leading to “phase mixing” of their distribution function and consequently to smoothing out of any “compressive” fluctuations (of density, pressure, etc.). This rapid mixing underlies Landau damping of these fluctuations in a quiescent plasma—one of the most fundamental physical phenomena that make plasma different from a conventional fluid. Nevertheless, broad power-law spectra of compressive fluctuations are observed in *turbulent astrophysical plasmas* (most vividly, in the solar wind) under conditions conducive to strong Landau damping. Elsewhere in nature, such spectra are normally associated with fluid turbulence, where energy cannot be dissipated in the inertial scale range and is therefore cascaded from large scales to small. By direct numerical simulations and theoretical arguments, it is shown here that turbulence of compressive fluctuations in collisionless plasmas strongly resembles one in a collisional fluid and does have broad power-law spectra. This “fluidization” of collisionless plasmas occurs because phase mixing is strongly suppressed on average by “stochastic echoes”, arising due to nonlinear advection of the particle distribution by turbulent motions. Besides resolving the long-standing puzzle of observed compressive fluctuations in the solar wind, our results suggest a conceptual shift for understanding kinetic plasma turbulence generally: rather than being a system where Landau damping plays the role of dissipation, a collisionless plasma is effectively dissipationless except at very small scales. The universality of “fluid” turbulence physics is thus reaffirmed even for a kinetic, collisionless system.

plasma turbulence | Landau damping | plasma echo | solar wind

What makes plasma turbulence a particularly fascinating subject is, apart from its ubiquity in the laboratory and in space, its kinetic nature. Plasma dynamics are six-dimensional, evolving in the phase space of positions and velocities,  $(\mathbf{r}, \mathbf{v})$ . Free energy that is injected at large scales must be transferred to small scales in  $\mathbf{r}$  or  $\mathbf{v}$  before it can be dissipated (see [1] and references therein). In nature, the range of scales implicated can be quite large, and the general theory is, therefore, a formidable challenge. At spatial scales larger than the Larmor radii of the particles, on time scales longer than those particles’ Larmor periods, and with account taken of the smallness of the electron mass relative to the ion mass, turbulent, magnetized plasma can be described by a reduced version [2] of the drift-kinetic, or “Kinetic-Magnetohydrodynamic” [3], approximation, whereby the phase space is reduced to four dimensions  $(\mathbf{r}, v_{\parallel})$ , where only the velocity  $v_{\parallel}$  parallel to the magnetic field survives as a kinetic variable. Even this simplified problem is manifestly kinetic in its nature, conceptually interesting and as yet unsolved.

In this regime, the transfer of free energy to small scales in phase space can be conceptualized as a superposition of two fundamental processes: *nonlinear* spatial mixing of the

fluctuating electric and magnetic fields, as well as of the particle distribution function, by the turbulent  $\mathbf{E} \times \mathbf{B}$  flows across the magnetic field, and *linear* phase mixing of the distribution function, brought about by particle streaming along magnetic-field lines. The former is *turbulence* in the usual “fluid” sense [4]. The latter, in the linear plasma theory, is known as *Landau damping*: it involves the transfer of free energy from the “fluid” quantities such as density, velocity, magnetic field, etc., to higher velocity moments of the perturbed distribution function (fine-scale structure in velocity space; see, e.g., [6–8]). How the “turbulent cascade” works in the presence of these two types of mixing is a fundamentally interesting question, which, with the advent of high-resolution measurements of turbulence in the solar wind [9, 10] and of kinetic simulations of this turbulence [11–17], has increasingly preoccupied theoreticians and modellers (indeed, not only in application to space plasmas, but also, for an even longer time, to fusion ones [7, 18–24]).

Because the computational resources required to solve the full, four-dimensional system (as we shall do here) are formidable and difficult to extend to realistic situations, several groups have taken a middle road, replacing the distribution function with a few of its  $v_{\parallel}$  moments. One must close the resulting fluid hierarchy in some fashion. “Landau-fluid” closures [6, 7, 20, 21, 25–29] enforce outgoing boundary conditions for free energy in the linearized equations, from resolved moments to unresolved. They thus model the transfer of energy to small scales in velocity space assuming that the energy carried to the higher resolved moments is ultimately dissipated

## Significance Statement

Two textbook physical processes compete to thermalize turbulent fluctuations in collisionless plasmas: Kolmogorov’s “cascade” to small spatial scales, where dissipation occurs, and Landau’s damping, which transfers energy to small scales in velocity space via “phase mixing”, also leading to dissipation. We show that, in a magnetized plasma, another textbook process, plasma echo, brings energy back from phase space and on average cancels the effect of phase mixing. Energy cascades effectively as it would in a fluid system and thus Kolmogorov wins the competition with Landau for the free energy in a collisionless turbulent plasma. This reaffirms the universality of Kolmogorov’s picture of turbulence and explains, for example, the broad Kolmogorov-like spectra of density fluctuations observed in the solar wind.

R.M., A.A.S., W.D., and A.K. conceived this project, including its theoretical rationale, and interpreted the results; A.K. carried out some preliminary numerical experiments and their analysis; R.M. wrote a new code and carried out the numerical simulations and data analysis presented in the paper; R.M., A.A.S., and W.D. wrote the paper.

The authors declare no conflict of interest.

<sup>1</sup>To whom correspondence should be addressed. E-mail: romain.meyrand@lpp.polytechnique.fr

by (very weak) collisions. An even more radically pragmatic modelling choice, popular in astrophysical applications, is to assume that the effect of phase mixing is merely to damp the spatial part of the turbulent cascade of the “fluid” quantities at a scale-dependent rate equal to the linear Landau damping rate in the system [30–34]. We shall see that the latter approach in general misses an essential property of turbulent plasma—but we shall give some credence to the notion that Landau-fluid models, carefully constructed, might capture the relevant physics.

In the context of solar-wind turbulence (and, more generally, of collisionless plasma turbulence, of which the solar wind is a particularly well-diagnosed instance), the question of how the turbulent fluctuations’ energy (free energy) is thermalized must be tackled if one is to explain the measured spectra of “compressive” (density and magnetic-field-strength) perturbations. In the fluid (short-mean-free-path) magnetohydrodynamic (MHD) theory, these perturbations correspond to the slow-wave and entropy modes. Compressions are supported in MHD by collisions, which prevent particles from freely streaming through and away, along the magnetic field. Because momentum and energy are conserved in each collision, the inertial-range fluctuations are undamped (viscosity and resistivity do dissipate them, but at much smaller spatial scales). Instead, they are passively advected by the Alfvénic perturbations, including in situations when the latter are turbulent [2, 35]. As passive tracers, compressive MHD perturbations should have a spectrum that follows the spectrum of the Alfvénic turbulence—and indeed solar-wind measurements show that they do [36–42]. However, the solar-wind plasma at 1 AU, where these measurements are done, is essentially collisionless: its mean free path is approximately 1 AU. In such a plasma, compressive perturbations, while still passive with respect to the Alfvénic ones [2], are in fact subject to Landau damping (known in this context as Barnes [43] damping) at rates characterized by free streaming along field lines. Thus, the variances of density and field-strength fluctuations are not conserved—they form part of the total compressive free energy, which includes also the variance of the perturbed ion distribution function and could be rapidly redistributed through all scales in velocity space—equivalently, to higher velocity-space moments—until it is ultimately dissipated by collisions. By this conventional argument, the wavenumber spectra of the compressive perturbations should decay more steeply in a collisionless plasma than in a collisional one, because at each scale, energy is removed into phase space at a rate at least similar to the rate at which it is passed to the next smaller scale.<sup>1</sup> Yet, this is not observed. Not only do the observed compressive fluctuations have spectra that follow the Alfvénic fluctuations’ spectra, as if the flow of free energy to higher moments were substantially blocked, they also display surprisingly “fluid” dynamics [46].

A range of possible explanations for this “fluid” behaviour of a collisionless plasma have been mooted: e.g., that Landau damping might be quantitatively weak [35], or that compressive fluctuations, unlike the Alfvénic ones, do not develop small scales along the (perturbed) magnetic field lines, ren-

dering the damping ineffective [2]. What in fact happens is subtler: while the compressive fluctuations do have a parallel cascade and thus do phase-mix vigorously, much of their energy flux into phase space due to this phase mixing is on average canceled by a return flux from phase space, due to the stochastic version [23] of the plasma echo phenomenon [47, 48]. The result is effective suppression of Landau damping of the compressive fluctuations. With access to this loss channel inhibited, the density and magnetic-field-strength perturbations instead develop increasingly sharp, small-scale spatial features, characterized by broad power-law wavenumber spectra. Their free energy is ultimately thermalized by processes that occur at small spatial scales (at and below the ion Larmor radius [2]), outside the scope of this study.

## Theoretical Framework

Motivated by observational evidence that turbulence in the solar wind consists of low-frequency fluctuations (compared to the ion Larmor frequency), with negligible energy in the fast magnetosonic modes, we tackle the problem in the framework of “Kinetic Reduced Magnetohydrodynamics” (KRMHD) [2], which is the long-wavelength limit of gyrokinetics [34, 49, 50] and the anisotropic reduction of Kinetic MHD [3, 51]. The electrons are isothermal in this approximation, so only the ions require a kinetic treatment. The collisional limit of KRMHD is the well-known “Reduced MHD” [52, 53].

The applicability of KRMHD is limited by a few constraints. Most importantly, these include magnetized ions ( $\lambda \gg \rho_i$ , where  $\rho_i$  is the thermal ion Larmor radius and  $\lambda$  is any target fluctuation’s scale length measured across the magnetic field); spatial anisotropy ( $\lambda \ll \ell_{\parallel}$ , where  $\ell_{\parallel}$  is a fluctuation’s scale length along the local magnetic field); and low frequency ( $\omega \ll \Omega$ , where  $\omega$  represents any dynamical frequency of interest and  $\Omega$  is the ion Larmor frequency). The fluctuating fields must be small in comparison to their background values (ordered  $\sim \omega/\Omega \sim \lambda/\ell_{\parallel}$ ), and the background magnetic field is assumed to be (locally) straight, with constant magnitude. The ion mean free path  $\lambda_{\text{mfp}}$  can be long or short compared to  $\ell_{\parallel}$  without violating KRMHD orderings. Similarly, the ratio of the sound speed to the Alfvén speed ( $\sim \sqrt{\beta_i}$ , where  $\beta_i$  is the ratio of the ion thermal to magnetic energies) can be large or small. KRMHD is well suited to the study of the inertial-range turbulence, in the solar wind and elsewhere.

Under this approximation, Alfvénic fluctuations are completely unaffected by the compressive fluctuations, and the compressive fluctuations are affected *only* by the Alfvénic fluctuations and not by one another [2].

**Alfvén waves.** In KRMHD, Alfvénic fluctuations are purely transverse, incompressible, nonlinearly interacting Alfvén-wave packets, which propagate in both directions along a straight, static background magnetic field  $\mathbf{B}_0 = B_0 \hat{\mathbf{z}}$ , in a plasma with mean mass density  $\rho_0$ . Two scalar stream (flux) functions  $\Phi = \Phi(\mathbf{r}, t)$  and  $\Psi = \Psi(\mathbf{r}, t)$  describe the fluctuating field-perpendicular flow velocity  $\mathbf{u} = \hat{\mathbf{z}} \times \nabla \Phi$  and magnetic field  $\mathbf{b} = \hat{\mathbf{z}} \times \nabla \Psi$ , respectively; the latter is in units of the Alfvén speed  $v_A = B_0/\sqrt{4\pi\rho_0}$ . Only the  $z$  components of the vorticity  $\nabla \times \mathbf{u}$  and current  $\nabla \times \mathbf{b}$  are non-zero, equal to  $\nabla_{\perp}^2 \Phi$  and  $\nabla_{\perp}^2 \Psi$ , respectively.

The Elsässer representation  $\mathbf{Z}^{\pm} = \mathbf{u} \pm \mathbf{b}$  [54] brings to the fore key features of Alfvénic fluctuations in full MHD.

<sup>1</sup>The damping rate of perturbations with parallel wave number  $k_{\parallel}$  is  $\sim |k_{\parallel}| v_{\text{th}}$ , where  $v_{\text{th}}$  is the ion thermal speed. The nonlinear cascade rate due to mixing of the compressive perturbations by the Alfvénic turbulence is, by the critical-balance conjecture [44, 45],  $\sim k_{\parallel} v_A$ , where the Alfvén speed is typically  $v_A \sim v_{\text{th}}$ . The steepening of the spectra in a turbulent system where the damping rate is comparable to the cascade rate at every scale is explained in Sec. 2.4.4 of [23].

In our reduced theory, the Elsässer potentials  $\zeta^\pm = \Phi \pm \Psi$  and “vorticities”  $\omega^\pm = \nabla_\perp^2 \zeta^\pm$  are useful. In terms of these functions, the KRMHD equations for Alfvénic fluctuations are

$$\left(\frac{\partial}{\partial t} \mp v_A \frac{\partial}{\partial z}\right) \omega^\pm = -\{\zeta^\mp, \omega^\pm\} - \{\partial_j \zeta^\mp, \partial_j \zeta^\pm\}, \quad [1]$$

where  $\{f, g\} \equiv \partial_x f \partial_y g - \partial_y f \partial_x g$ . In the final term in equation 1, summation over  $j = x, y$  is implied.

Important Alfvénic phenomena are easily read from equation 1. The linear terms (on the left-hand side) describe perturbations propagating up and down the background magnetic field with speed  $v_A$ . According to the right-hand side, only counter-propagating perturbations interact. The compressive fluctuations do not appear. Note that the local *direction* of the magnetic field is determined by the Alfvén waves, because  $\mathbf{B}/B \approx \hat{\mathbf{z}} + \mathbf{b}/v_A$ . KRMHD separately tracks fluctuations of the magnetic-field *strength*,  $\delta B$ , as described below.

**Ion kinetics.** Compressive fluctuations, namely those of density ( $\delta n$ ) and pressure, are calculated via moments of the ion distribution function perturbed from a Maxwellian equilibrium; the perturbed magnetic-field strength  $\delta B$  is obtained from these via pressure balance (across the mean field  $\mathbf{B}_0$ ). In KRMHD, as a result of the straight- $\mathbf{B}_0$  equilibrium geometry, magnetic-moment conservation, and the restriction to long wavelengths ( $\lambda \gg \rho_i$ ), one can integrate the perturbed distribution function over perpendicular velocities  $v_\perp$ , retaining only the  $v_\perp^0$  and  $v_\perp^2$  moments, which are required to obtain  $\delta n$  and  $\delta B$ . The ion kinetics are thus encoded by two kinetic scalar fields,  $g = g^{(i)}(\mathbf{r}, v_\parallel, t)$ ,  $i = 1, 2$ , which are particular linear combinations of the  $v_\perp^0$  and  $v_\perp^2$  moments, chosen to produce two decoupled kinetic equations [2]:

$$\frac{dg^{(i)}}{dt} + v_\parallel \nabla_\parallel g^{(i)} + v_\parallel F_0 \nabla_\parallel \phi^{(i)} = 0, \quad [2]$$

where  $F_0 = \exp(-v_\parallel^2/v_{th}^2)/\sqrt{\pi}v_{th}$  is the background Maxwellian distribution. Ions are accelerated along the moving field lines by the parallel electric field and the mirror force. For each  $g^{(i)}$ , the appropriate linear combination of these forces is accounted for by its potential  $\phi^{(i)} = \alpha^{(i)} \int dv_\parallel g^{(i)}(v_\parallel)$ , where the constant prefactors  $\alpha^{(i)}$  depend on plasma parameters—the ratios of ion thermal to magnetic energies (“plasma beta”,  $\beta_i \equiv 8\pi n_i T_i/B_0^2$ ), of the ion to electron temperatures,  $\tau \equiv T_i/T_e$ , and of the ion to electron charge,  $Z \equiv q_i/|e|$ . The explicit expressions are  $\alpha^{(i)} = (\tau/Z - 1/\beta_i \pm \kappa)^{-1}$ , with “+” for  $i = 1$  and “−” for  $i = 2$  and  $\kappa = [(1 + \tau/Z)^2 + 1/\beta_i^2]^{1/2}$ . At any time and location,  $\delta n$  and  $\delta B$  can be determined as linear combinations of  $\phi^{(1)}$  and  $\phi^{(2)}$ , with coefficients that also depend on the plasma parameters:

$$\frac{\delta n}{n_i} = \frac{1}{2\kappa} \left[ \sigma \frac{\phi^{(1)}}{\alpha^{(1)}} - \frac{2\tau}{Z\beta_i} \frac{\phi^{(2)}}{\alpha^{(2)}} \right], \quad [3]$$

$$\frac{\delta B}{B_0} = \frac{1}{2\kappa} \left[ \sigma \frac{\phi^{(2)}}{\alpha^{(2)}} - \left(1 + \frac{Z}{\tau}\right) \frac{\phi^{(1)}}{\alpha^{(1)}} \right], \quad [4]$$

where  $\sigma = 1 + \tau/Z + 1/\beta_i + \kappa$ . The particular forms of these coefficients or of  $\alpha^{(i)}$  are not important for the forthcoming discussion, which hinges just on the mathematical structure of equation 2. We shall drop the superscripts of  $g$  and  $\phi$  wherever this causes no ambiguity.

The apparent simplicity of equation 2 is an intentional feature of the KRMHD model, but a few subtleties deserve

mention. The equations for  $g^{(1)}$  and  $g^{(2)}$  are totally decoupled from one another, but not from the background Alfvénic perturbations, which move the plasma and the field lines around. This effect enters via the “convective” derivatives  $d/dt \equiv \partial/\partial t + \mathbf{u} \cdot \nabla_\perp$  and  $\nabla_\parallel \equiv \partial/\partial z + (\mathbf{b}/v_A) \cdot \nabla_\perp$ .

In the presence of Alfvénic fluctuations, since the magnetic field lines are “frozen” into the plasma, the Alfvénic flows  $\mathbf{u}$  move the field lines  $\mathbf{b}$  and the plasma together. Thus, equation 2 might seem to be a linear equation that has been re-expressed in a well-defined Lagrangian frame [2]. However, after about one eddy-turnover time, structure in  $\mathbf{b}$  develops at arbitrarily small spatial scales [55–57]. Thus, in the presence of any resistivity (not shown in equation 1, but included in our simulations and in reality), the field lines’ identities and thus the Lagrangian frame are lost. Consequently, a density fluctuation (for example) that is momentarily aligned with the local magnetic field develops finer parallel wavelengths in about one eddy-turnover time.<sup>2</sup> This process of field-line dissolution and replacement manifests as a forward parallel cascade of compressive fluctuations by background Alfvénic fluctuations, as we observe in our simulations (see figure 3).

The derivative operators in equation 2 are independent of  $v_\parallel$  and the  $v_\parallel$  integrals extend from  $-\infty$  to  $+\infty$ . These properties and the appearance of the Maxwellian function  $F_0(v_\parallel)$  make Hermite polynomials a natural orthogonal basis for  $g(v_\parallel)$ . That is, one can decompose

$$g(v_\parallel) = \sum_{m=0}^{\infty} \frac{H_m(v_\parallel/v_{th})F_0(v_\parallel)}{\sqrt{2^m m!}} g_m, \quad [5]$$

where  $H_m(x) = (-1)^m e^{x^2} (d/dx)^m e^{-x^2}$  is the Hermite polynomial of degree  $m$ . It is convenient to describe the velocity-space structure of  $g(v_\parallel)$  in terms of the spectral coefficients  $g_m$ . Just as a fluid cascade is described in terms of a flux of energy from low to high wavenumbers, one may describe collisionless damping as a flux of free energy from low  $m$  to high  $m$ .

In this context, it is appropriate to state explicitly what we mean by free energy [2]. It follows immediately from equation 2 that it has a quadratic invariant:

$$W = \int \frac{d^3\mathbf{r}}{V} \left( \int dv_\parallel \frac{g^2}{2F_0} + \frac{\phi^2}{2\alpha} \right) = \frac{1}{2} \sum_{\mathbf{k}} \left( \sum_{m=0}^{\infty} |g_{m,\mathbf{k}}|^2 + \alpha |g_{0,\mathbf{k}}|^2 \right), \quad [6]$$

where  $V$  is the volume of the domain and the second expression follows from the Parseval theorem for the Fourier and Hermite functions and provides an explicit motivation for discussing free-energy flows in the  $(m, \mathbf{k})$  phase space. It is not hard to show that  $W$  is minus the entropy of the perturbed distribution plus the energy of the fluctuating magnetic field (up to a factor of  $T_i$ ), which is what motivates the term “free energy”.

<sup>2</sup>Note that, absent resistivity, the parallel electric field associated with Alfvénic fluctuations is zero, and one might therefore mistakenly believe that the potentials  $\phi$  describe all parallel electric fields also in resistive KRMHD. In fact, the moving field lines associated with the Alfvénic fluctuations can change their topology in the presence of resistivity and generate parallel electric fields in the process. In KRMHD, the compressive fluctuations cannot see these resistive parallel electric fields; they are not included in  $\phi$ . Thus, when field lines resistively reconnect, KRMHD compressive fluctuations are undisturbed, but get relabeled as the field-line identities change. It is this relabeling that causes the compressive fluctuations to inherit the parallel structure of the Alfvénic fluctuations.

**Landau damping, phase mixing and stochastic echo.** In the absence of Alfvénic fluctuations, equation 2 is the one-dimensional, unmagnetized problem originally considered by Landau [5], so the compressive fields  $\phi$  are subject to his damping. In the presence of Alfvénic turbulence, the rate of collisionless damping is *enhanced*, because the damping rate and the associated rate of formation of structure in velocity space are proportional to  $|k_{\parallel}|v_{\text{th}}$ , which is *increased* by the parallel cascade of compressive fluctuations. If this were the end of the story, i.e., if the compressive-fluctuation spectra were determined solely by simple “superposition” of the turbulent cascade and Landau damping, then one would predict steep (and possibly non-universal) Fourier spectra [23, 58] and shallow Hermite spectra [8, 59], corresponding to free energy spreading to small scales in velocity space as quickly as to small scales in real space. But there is more to the story.

In the absence of collisions, phase mixing is formally reversible. Spatial perturbations of fields  $\phi$  decay in time as spatial perturbations of the distribution function are transferred to finer scales in velocity space (higher Hermite moments  $g_m$ ), but until collisions scramble the phases, the process can in principle be reversed. Consider equation 2 for an initial value problem, with the initial perturbation  $\phi(\mathbf{r}_{\perp}, \ell) \sim \cos(k_{\perp}\ell)$  along some field line labeled by the perpendicular coordinate  $\mathbf{r}_{\perp}$ . If we could Fourier transform  $g(\mathbf{r}_{\perp}, \ell, v_{\parallel}, t)$  along the moving field line, we would find the ballistic (or “free-streaming”) part of the response to be  $g_{k_{\parallel}} \sim \exp(-ik_{\parallel}v_{\parallel}t)$ ; the argument of the exponent is the “phase” in “phase mixing”. The “mixing” occurs when one integrates  $g_{k_{\parallel}}(v_{\parallel})$  over  $v_{\parallel}$ , as one would to find a self-consistent  $\phi$ —the Maxwellian velocity dependence of  $F_0(v_{\parallel})$  in the initial condition is then mixed with the perturbation’s advancing phase [6, 7]. A more complete analysis is required to recover Landau’s full story, but the essential connection between phase mixing and the damping of fields that is exposed here is authentic. Velocity-space integrals decay even as  $g_{k_{\parallel}}(v_{\parallel})$  itself only becomes more oscillatory in  $v_{\parallel}$ , without decaying. If time were reversed, the accumulated phase would unmix, and the original  $\phi$  perturbations would grow in time, until the unmixing were complete.

It is not easy to reverse time, but the scattering of a compressive wave by an Alfvén wave that is propagating in the opposite direction along the field line has the same mathematical effect: such an interaction causes the compressive wave’s  $k_{\parallel}$  to change sign, the phase subsequently unmixes and the field perturbation regenerates. The most familiar example of this phase unmixing is the textbook phenomenon of plasma echo [47, 48]. The idea of a stream of stochastic echoes produced by a sequence of nonlinear interactions has been the object of several recent studies of *electrostatic* ( $\mathbf{b} = 0$ ) plasma turbulence [23, 24, 60, 61]. Here, we explore for the first time the possibility of stochastic echoes in a plasma with moving field lines ( $\mathbf{b} \neq 0$ ). As described above, the compressive fluctuations couple to the Alfvénic fluctuations in a nontrivial way, as the field lines along which the particles stream are being advected by the same flows as the particles’ distribution function  $g$ . Although there is as yet no complete theory for this problem, our numerical results suggest that elements of the electrostatic theory [23, 61] are germane. This generalization opens the way to understanding kinetic turbulence in heliospheric (solar-wind) and similarly collisionless astrophysical plasmas, which are usually well into the electromagnetic regime.

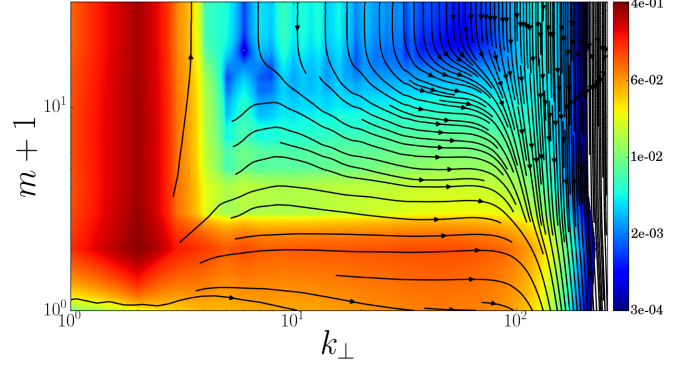


**Fig. 1.** The flux ( $\Pi, \Gamma$ ) (see equations 9 and 11) of free energy  $W$  (equation 6) of the kinetic field  $g^{(1)}$ , normalized to its injection rate, as a function of the Hermite number  $m$  (vertical) and perpendicular wavenumber  $k_{\perp}$  (horizontal). Colors represent the magnitude of the flux and arrows its streamlines. Away from the stirring (at small  $m$  and small  $k_{\perp}$ ) and damping (at large  $m$  and/or large  $k_{\perp}$ ), the time-averaged net turbulent free-energy flux to high  $m$  is very small; Landau damping is largely suppressed by stochastic echoes (return flux from high to low  $m$ ) and so different Hermite moments  $g_m$  of the ion distribution function are effectively energetically insulated from each other.

Below we show evidence that nonlinear, stochastic echoes are present, and that they can have profound effects on observable quantities. Our key finding, best illustrated by figure 1, is that in the inertial range, the average net flux of free energy to smaller velocity-space scales (higher Hermite moments) is very small in comparison with the average net flux of free energy to smaller spatial scales (higher perpendicular wavenumbers). In the figure, this conclusion is supported by the nearly horizontal stream lines of the flux in the inertial range (away from the stirring at long wavelengths and from the dissipation at the smallest scales). After a brief discussion of the set up of our numerical experiment, we provide further evidence from the simulations, including detailed spectra and structure functions such as can be (or have been) obtained from solar-wind measurements.

## Numerical Experiment

**Numerical set up.** Our simulations track the evolution of driven and damped compressive fluctuations in a sea of driven and damped Alfvénic turbulence for a number of the latter’s eddy-turnover times—well into the statistically stationary state, so statistical averages can be reliably calculated.

We solve equations 1 and 2 spectrally in Fourier–Hermite space. Namely, we solve equation 2 in the form of a number of coupled “fluid” equations for the Hermite moments  $g_m$ , defined by equation 5:

$$\frac{dg_m}{dt} + v_{\text{th}} \nabla_{\parallel} \left[ \sqrt{\frac{m+1}{2}} g_{m+1} + (1 + \alpha \delta_{m,1}) \sqrt{\frac{m}{2}} g_{m-1} \right] = 0 \quad [7]$$

and  $\phi = \alpha g_0$ . We advance these equations in time with a third-order modified Williamson algorithm (a four-step, low-storage Runge-Kutta method). The spatial dependence of all fields is expressed as discrete Fourier series and we use the standard pseudo-spectral approach to solve the linear and nonlinear terms containing spatial derivatives. The simulation domain is

a triply periodic cube of size  $2\pi$  in each direction.<sup>3</sup> The code units are set by this and by  $v_A = 1$ . The nonlinear terms are partially dealiased using a phase-shift method [62]. The total number of spectral modes is therefore smaller than the total number of mesh points used to evaluate the nonlinear terms; we report the spatial size of a given simulation in terms of the latter. The simulations presented here have spatial resolution from  $256^3$  (figure 4) to  $512^3$  (all figures).

The description of compressive fluctuations provided by equation 2 is appropriate for the inertial range, but the *production* of fluctuations at large scales and their removal at small scales in a simulation require one to add forcing and dissipation, respectively. The forcing occurs at  $m = 1$  and low wavenumbers, viz.,  $|k_x|, |k_y|, |k_z| = 1, 2$ . The strength of the forcing can be arbitrary because equation 2 is linear in  $g$  and so the amplitude of the compressive fluctuations is arbitrary. Our forcing is designed so as to keep the rate of injection of the compressive free energy exactly constant.

We add two forms of dissipation to equation 2, to absorb energy at small scales in  $\mathbf{r}$  (“hyperviscosity”) and  $v_{\parallel}$  (“hypercollisionality”) without changing the dynamics at large scales. We tested multiple specific forms of dissipation in the course of this study. Our results require the presence of the dissipation at small scales, but do not depend on its specific form. In the simulations reported here, we add  $-\mu k_{\perp}^8 g_m - \nu m^6 g_m$  to the right-hand side of equation 7 with  $m \geq 2$ . The values of  $\mu$  and  $\nu$  are chosen so that this dissipation is significant only for modes with the largest values of  $k_{\perp}$  and  $m$  but removes energy without creating bottlenecks or reflections.

In practice, the Hermite series of  $g(v_{\parallel})$  (equation 5) is truncated at some  $m = M$ . In the absence of collisions, the Hermite equations 7 fail to close, because the evolution of each  $g_m$  depends on  $g_{m+1}$  (and  $g_{m-1}$ ). However, with the hypercollisional cutoff described above, one can take  $g_{M+1} = 0$  to a very good approximation as long as  $M$  is chosen large enough. This is our approach. The simulations reported here have resolution from  $M = 32$  (all figures) to  $M = 128$  (figure 4).

The Alfvén waves are also stirred and damped. We stir them by forcing at low wavenumbers (the same as for the kinetic field  $g$ ) and in the velocity field only. The forcing is designed to keep the injected power  $\epsilon$  exactly constant, while maintaining the rate of cross-helicity injection exactly zero [63]. The magnitude of  $\epsilon$  allows us to control the character of the resulting Alfvénic turbulence: weaker injection produces weakly interacting Alfvén waves, but increasing it pushes the system towards strong, critically balanced turbulence [44, 45]. This is the relevant regime that we study here. It is achieved when  $\epsilon = 1$  in code units. Like the kinetic field, the Alfvénic fields are also dissipated by eighth-order “hyperviscosity” and “hyperresistivity”, artificially set to be numerically equal.

The plasma parameters  $\beta_i$ ,  $\tau$  and  $Z$  are all set to unity. They enter via the constants  $\alpha^{(i)}$  in the definitions of the potentials  $\phi^{(i)}$  in terms of  $g^{(i)}$  and affect their Landau-damping rates. They are also needed to compute the relative amplitudes of  $\delta n$  and  $\delta B$ , via equations 3 and 4. The results presented here do not depend significantly upon these as long as they

<sup>3</sup>Note that in KRMHD, there is a rescaling symmetry whereby all fluctuation amplitudes relative to the corresponding background values (e.g.,  $\delta B/B_0$ ,  $u/v_A$ ,  $g/F_0$  etc.) can be arbitrarily rescaled as long as the ratios of all perpendicular to parallel scales are rescaled by the same amount (i.e., the fluctuation amplitudes and  $k_{\parallel}/k_{\perp}$  are arbitrarily small). Therefore, the parallel and perpendicular units of length are independent.

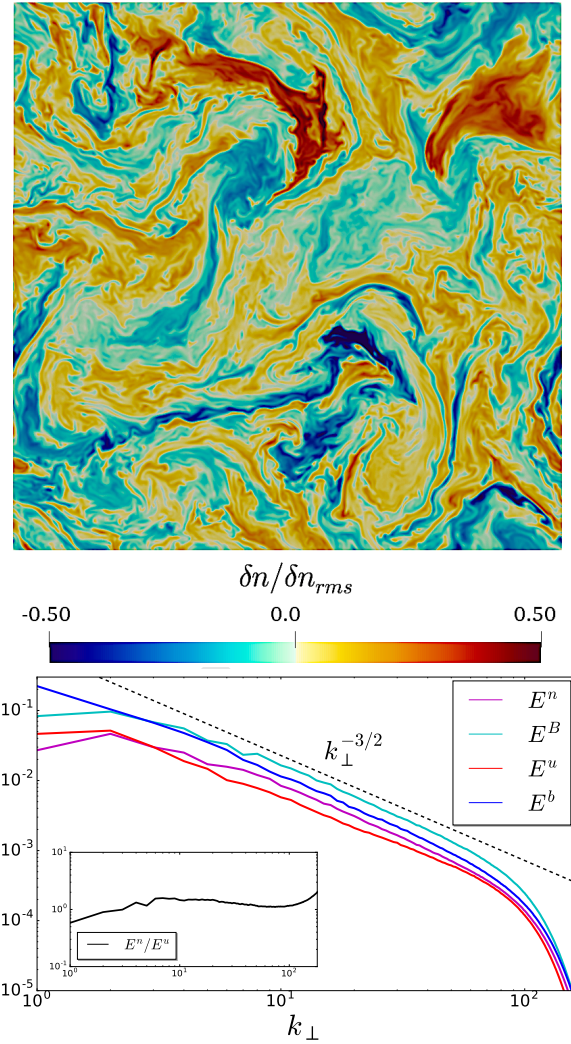


**Fig. 2. Perpendicular cascade.** Upper panel: snapshot of the density-fluctuation field  $\delta n$  in the plane  $(x, y)$  perpendicular to the mean magnetic field. Lower panel: perpendicular spectra of the Alfvénic (velocity  $E^u$  and magnetic  $E^b$ ), density ( $E^n$ ) and magnetic-field-strength ( $E^B$ ) fluctuations; inset: ratio of the density to Alfvénic-velocity spectra,  $E^n/E^u$ . The Alfvénic spectra are normalized to the total mean Alfvénic energy, compressive spectra to the total mean free energy  $W$  (equation 6).

are all  $\sim 1$ .

**Perpendicular spectra.** Let us first establish that we are dealing with a system that exhibits some familiar features of turbulence.

A snapshot of the density-fluctuation field in the plane perpendicular to the background magnetic field is shown in figure 2, together with time-averaged perpendicular wavenumber spectra of the density  $\delta n$  ( $E^n$ ), magnetic-field strength  $\delta B$  ( $E^B$ ), and of the Alfvénic fluctuations of velocity  $\mathbf{u}$  ( $E^u$ ) and magnetic field  $\mathbf{b}$  ( $E^b$ ). The spectral slope of the latter follows quite well the  $k_{\perp}^{-3/2}$  scaling expected for RMHD turbulence [64–68]. To a good approximation, the compressive fluctuations’ spectra track the Alfvénic-velocity spectrum (see inset of figure 2), as one might expect an undamped passive scalar to do [69, 70]. We do not observe a significant steepening of the compressive spectra compared to the Alfvénic ones, which would have had to happen had there been Landau damping

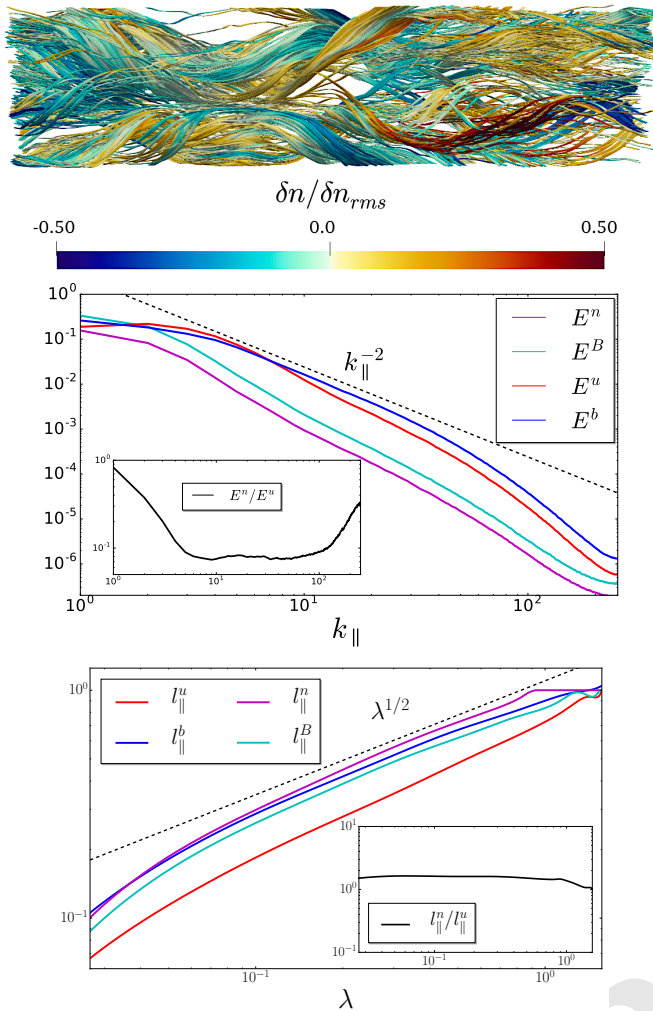


**Fig. 3. Parallel cascade.** Upper panel: snapshot of a typical set of magnetic-field lines, with color showing the density-fluctuation field. The  $z$  dimension of the box is lengthened by the factor of 4 for better viewing (formally, in KRMHD, it is arbitrarily longer than the perpendicular size of the box). Middle panel: parallel spectra of the Alfvénic, density and field-strength fluctuations, measured along perturbed field lines; inset: ratio of the density to Alfvénic-velocity spectra,  $E^n/E^u$ . The normalizations are the same as in figure 2. Lower panel: parallel coherence length  $\ell_{\parallel}$  of Alfvénic, density and field-strength fluctuations as a function of their perpendicular coherence length  $\lambda$ ; inset: ratio of the parallel coherence length of the density to that of the Alfvénic velocity. Here  $\ell_{\parallel}(\lambda)$  is calculated via the second-order correlation function, by the method described in [71], but following the perturbed field lines with higher-order accuracy, as described in the text.

of compressive fluctuations depleting their energy cascade at each scale [23]. This is circumstantially consistent with an inhibition of Landau damping. It is also essentially consistent with what is observed in the solar wind [36–42].

**Existence of parallel cascade.** Critically balanced Alfvénic fluctuations become progressively more anisotropic at finer scales [44, 45], with parallel and perpendicular correlation scales related by  $\ell_{\parallel} \propto \lambda^{1/2}$  [64, 65, 71]. Consequently, their parallel spectrum is expected to scale as  $k_{\parallel}^{-2}$  [45, 65, 72] (and indeed does in the solar wind [9, 67, 73–75]). The question that we address here is whether the kinetic field  $g$  advected by them “inherits” this parallel cascade.

Because  $\ell_{\parallel} \gg \lambda$ , parallel correlations can only be measured correctly along the *fluctuating* field [66, 67, 76]. We identify the field lines by tracing a set of them from 100,000 randomly chosen points in the simulation domain at a given instant in

time, record the values of fluctuating quantities as functions of the distance along each field line, and then calculate parallel spectra (we use a fourth-order Runge-Kutta method to integrate the field lines and cubic spline interpolation to determine values of the fluctuating fields on them).

The results from this analysis are shown in figure 3 alongside an instantaneous snapshot of field lines, in which they are “painted” with the values of the density-fluctuation field. One can see that the field lines wander widely across the domain. The resulting parallel wavenumber spectra are steeper than the perpendicular wavenumber spectra, as expected. The  $k_{\parallel}^{-2}$  scaling is well satisfied for  $E^b$ , whereas the Alfvénic-velocity spectrum  $E^u$  is a little steeper. The compressive spectra closely track  $E^u$  (see inset), confirming the existence of a “parallel cascade” of these passive fields (contrary to what was believed by [2] on the basis of linearity of equation 2 in a suitably well-behaved Lagrangian frame). The lower panel of figure 3 reinforces this conclusion: the parallel coherence lengths of the compressive fluctuations scale as  $\lambda^{1/2}$ , as do those of the Alfvénic fluctuations.

The existence of a parallel cascade is an important finding of the present study. As we have argued above, it occurs because magnetic fields reconnect at every scale over a time comparable to the correlation time associated with this scale [55–57] and thus cannot preserve their identity over more than one parallel correlation scale of the Alfvénic turbulence—thus, any density perturbation that extends along a field line will be broken up and decorrelated on the same parallel scale (hence the tracking of the Alfvénic spectra by the compressive ones).

It is the presence of the parallel cascade that makes the question of the efficiency of Landau damping relevant: its rate  $\sim |k_{\parallel}|v_{\text{th}}$  will be of the same order as the Alfvén frequency  $k_{\parallel}v_A$  (taking  $\beta_i = 1$ ) and so, in a critically balanced turbulence, of the same order as the nonlinear cascade rate at every scale. It therefore *a priori* matters as an energy-removal channel and the discovery that it in fact does not is a nontrivial one.

**Phase-space spectra and dissipation.** Let us now complete the characterisation of the free-energy distribution in phase space by studying the structure of the fluctuations of  $g$  in velocity space, in terms of its Hermite spectra. Besides helping us build our case for fluidization of kinetic turbulence, these are of interest in the context of the rapid recent advances in both instrumentation and computing, meaning that they can now be measured directly both in space [10] and in fully kinetic simulations [14, 17, 77].

In the absence of background Alfvénic turbulence, the time- and space-averaged Hermite spectrum of a forced and Landau-damped kinetic field is  $\langle |g_m|^2 \rangle \propto m^{-1/2}$  [8, 59]. This corresponds to a constant finite free-energy flux from small to large Hermite numbers. As a consequence, there is a dissipative anomaly associated with the collision operator: in the limit of vanishing collisionality, the collisional dissipation stays finite, enabling the removal of free energy from the system at a collisionality-independent phase-mixing rate. With turbulence, we find the spectrum to be a little steeper than  $m^{-1}$ , as shown in figure 4. Collisional dissipation rate associated with such a spectrum would vanish in the limit of small collisionality [61], indicating that refinement of scales in velocity space is not sufficient to process into heat the finite free energy injected by forcing, and thus that the principal cascade route must

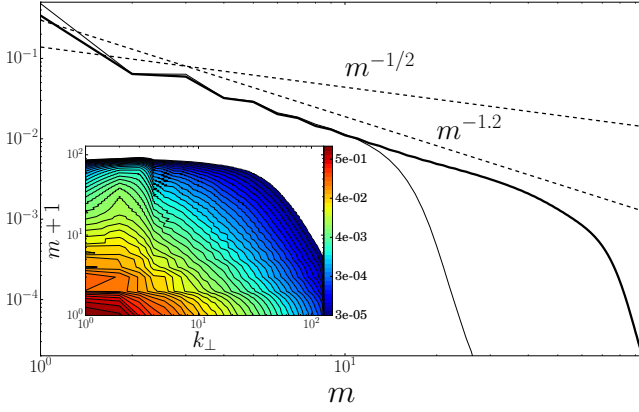


**Fig. 4. Phase-space cascade.** Hermite spectrum (integrated over wavenumbers) of the kinetic field  $g^{(1)}$  advected by Alfvénic turbulence according to equation 2: the thick line shows the spectrum for a run with spatial resolution  $256^3$  and  $M = 128$  Hermite moments; the thin line is for a run with spatial resolution  $512^3$  and  $M = 32$  Hermite moments. The slope  $m^{-1/2}$  associated with linear Landau damping [8, 59] is shown for reference. The normalization of the spectrum is the same as in figure 2. Inset: spectrum of  $g^{(1)}$  in the phase space  $(k_{\perp}, m)$  (integrated over  $k_z$ ).

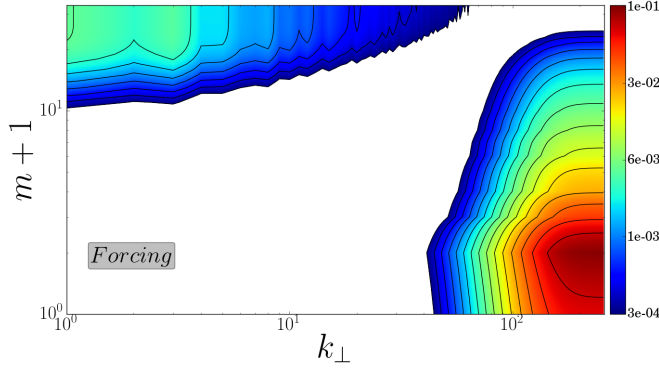


**Fig. 5.** Dissipation rate of the free energy  $W$  (defined by equation 6) of the kinetic field  $g^{(1)}$ , normalized to its total injection rate, as a function of the Hermite number  $m$  and perpendicular wavenumber  $k_{\perp}$ . Dissipation is important only for large  $m$  (hypercollisional) or large  $k_{\perp}$  (hyperviscous). In the inertial range, the free energy is well conserved. The range of  $(k_{\perp}, m)$  into which energy is injected by forcing is shown as grey box. Some of the energy injected at  $m = 1$  and low  $k_{\perp}$  is dissipated by collisions, but the dissipation is most intense at high  $k_{\perp}$  and low  $m$ .

be via smaller *spatial* scales. Indeed, figure 5, where we show the combined collisional and hyperviscous dissipation in the  $(k_{\perp}, m)$  phase space, confirms that the majority of the free energy is thermalized at small spatial scales, not at high  $m$ .

**Free-energy fluxes.** Finally, having collected all this circumstantial (but observationally testable) evidence for the “fluidization” of kinetic turbulence, let us return to figure 1, where the fluxes of free energy in the  $(k_{\perp}, m)$  space are plotted. Comparison of the fluxes towards smaller scales in velocity space (higher Hermite numbers) with the fluxes towards smaller scales in position space (higher wavenumbers) provides the most direct numerical evidence supporting the claim that, in the inertial range, Landau damping is suppressed rather than enhanced.

The compressive free energy,  $W$ , defined by equation 6, is conserved in the inertial range of our simulations. Indeed, forcing is implemented spectrally (in  $m$  and  $k_{\perp}$ ) and is, therefore,

exactly zero outside of a few lowest modes. The dissipation rate (shown in figure 5) is negligibly small away from the highest resolved  $m$  and  $k_{\perp}$ . For most  $m$  and  $k_{\perp}$  modes, there are, therefore, neither sinks nor sources of free energy other than coupling to other modes. Fluxes from mode to mode can then be defined in such a way that the free energy in a wavenumber shell  $|\mathbf{k}'_{\perp}| = k_{\perp}$  and at Hermite number  $m$ ,  $W_m(k_{\perp}) = \sum_{k'_z} \sum_{|\mathbf{k}'_{\perp}|=k_{\perp}} (1 + \alpha \delta_{m,0}) |g_{m,\mathbf{k}'}|^2 / 2$ , satisfies, away from the forcing and dissipation,

$$\frac{\partial W_m(k_{\perp})}{\partial t} = -[\Gamma_m(k_{\perp}) - \Gamma_{m-1}(k_{\perp})] - \frac{\partial \Pi_m(k_{\perp})}{\partial k_{\perp}}, \quad [8]$$

where  $\Gamma_m(k_{\perp})$  is the Hermite flux and  $\Pi_m(k_{\perp})$  is the Fourier flux. The Hermite coupling is essentially local (it involves only neighboring Hermite numbers  $m - 1$ ,  $m$  and  $m + 1$ ), and so it is easy to read off Hermite fluxes from equation 7:

$$\Gamma_m(k_{\perp}) = v_{\text{th}} \sum_{m'=0}^m \int \frac{d^3 \mathbf{r}}{V} (1 + \alpha \delta_{m',0}) [g_{m'}]_{k_{\perp}}^{\bar{}} \\ \nabla_{\parallel} \left[ \sqrt{\frac{m'+1}{2}} g_{m'+1} + (1 + \alpha \delta_{m',1}) \sqrt{\frac{m'}{2}} g_{m'-1} \right], \quad [9]$$

where the Fourier ring filter applied to a function is defined by

$$[g_m]_{k_{\perp}}^{\bar{}}(\mathbf{r}) = \sum_{k'_z} \sum_{|\mathbf{k}'_{\perp}|=k_{\perp}} e^{i\mathbf{k}' \cdot \mathbf{r}} g_{m,\mathbf{k}'}. \quad [10]$$

Fluxes in Fourier space can be nonlocal, but are commonly defined and studied nonetheless [78]:

$$\Pi_m(k_{\perp}) = (1 + \alpha \delta_{m,0}) \frac{2\pi}{\sqrt{L_x L_y}} \int \frac{d^3 \mathbf{r}}{V} [g_m]_{k_{\perp}}^{\geq} \mathbf{u} \cdot \nabla_{\perp} [g_m]_{k_{\perp}}^{\leq}, \quad [11]$$

where  $L_x L_y = (2\pi)^2$  is the cross-section of the box and the high- and low-pass Fourier filters are defined by

$$[g_m]_{k_{\perp}}^{\geq}(\mathbf{r}) = \sum_{k'_z} \sum_{|\mathbf{k}'_{\perp}| > k_{\perp}} e^{i\mathbf{k}' \cdot \mathbf{r}} g_{m,\mathbf{k}'}, \quad [12]$$

$$[g_m]_{k_{\perp}}^{\leq}(\mathbf{r}) = \sum_{k'_z} \sum_{|\mathbf{k}'_{\perp}| \leq k_{\perp}} e^{i\mathbf{k}' \cdot \mathbf{r}} g_{m,\mathbf{k}'}. \quad [13]$$

While the two-dimensional phase-space flux  $(\Pi, \Gamma)$  is not a unique quantity, defined up to arbitrary circulations in the  $(k_{\perp}, m)$  space, it is a useful one and, absent any obviously spurious such circulations, it gives a good representation of the paths that free energy takes to cross the gap between the forcing and dissipation scales.

It is  $(\Pi, \Gamma)$  vs.  $(k_{\perp}, m)$ , as defined by equations 11 and 9, that is plotted in figure 1. On average, at forcing scales (low  $k_{\perp}$ ), a significant amount of free energy flows directly to high  $m$ . This flux is restricted to the forcing band of  $k_{\perp}$  modes, because in this range, the nonlinear interactions have not yet managed to set up a return echo flux. This is in sharp contrast with the situation in the inertial range, where the energy flows mostly to small spatial scales. Recall that in the inertial range, the parallel cascade of compressive fluctuations should make Landau damping *stronger* in the presence of turbulence than otherwise, because free-streaming particles have less distance to travel to smooth out spatial fluctuations. Recall also that this parallel cascade is critically balanced, which means that

Landau damping should be able to “keep up” with nonlinear, spatial mixing at every scale in the inertial range. In reality (as represented by the simulations), Landau damping is manifestly rapid enough to be important at forcing scales but (on average) far weaker than perpendicular spatial mixing in the inertial range, so it is reasonable to conclude that there is another process that is cancelling on average the flux to high  $m$ . This is the most explicit signature of stochastic echoes that can be diagnosed in these simulations.<sup>4</sup>

The conclusion from figure 1 is that, in the inertial range, individual Hermite moments are, in effect, energetically insulated from each other, on average. The compressive turbulence is “fluidized”.

## Discussion

**Summary.** We have presented a case for effective fluidization of compressive fluctuations in collisionless (or weakly collisional) plasma turbulence. Compressive fluctuations are advected passively by the ambient Alfvénic turbulence and turn out to inherit its parallel structure (figure 3). This means that their phase-mixing (Landau-damping) rate  $\sim |k_{\parallel}|v_{\text{th}}$  is in principle comparable to the frequency  $k_{\parallel}v_A$  of the Alfvénic motions and, therefore, in a critically balanced turbulence [44, 45], to the rate at which these motions push the compressive free energy to smaller perpendicular scales. However, what might have been thought an effective dissipation at every scale fails to remove energy efficiently from the low-order moments of the ion distribution function (figure 1) and thus steepen the inertial-range spectra of, e.g., density and magnetic-field-strength fluctuations. Instead, they follow faithfully the spectrum of the advecting Alfvénic field (figure 2) as a well-behaved “fluid” passive scalar would do [69, 70]. The reason for this turns out to be that nonlinear advection effectively nullifies phase mixing (except at the forcing scales), with free-energy fluxes in the inertial range largely confined within each moment of the distribution function, taking its energy from large to small *spatial* scales, where it dissipates (figure 5). We interpret this behavior as resulting from statistical cancellation of phase mixing by plasma echoes. These are excited because the nonlinear advection causes phase-mixing modes propagating towards smaller velocity-space scales to couple to anti-phase-mixing ones, propagating back to larger scales—the result is a return flux from phase space [23].

**Relation to observations in space.** There is a long history of density and field-strength spectra being measured in the solar wind and found to have the same slopes as the ambient Alfvénic turbulence [36–42]. Why they do so in a collisionless plasma has remained a puzzle, if perhaps not always a fully appreciated one, in view of the community’s instinctive preference for fluid models. As solar wind has come to be regarded as a unique plasma physics laboratory, compressive fluctuations, under further, more plasma-physics-aware, scrutiny, have stubbornly continued to manifest “fluid” behavior [46]. Ours is the first dedicated attempt to simulate these fluctuations drift-kinetically, using equations that are physically appropriate for

<sup>4</sup>For electrostatic kinetic turbulence, where  $\mathbf{b} = 0$ , it is possible to decompose  $g_m$  explicitly into phase-mixing and anti-phase-mixing components and thus calculate directly the “forward” and “backward” free-energy fluxes in Hermite space [23, 61]. However, this decomposition involves the sign of  $k_{\parallel}$ , which in our case would have to be calculated with respect to the perturbed, turbulent magnetic field. We do not know how to make such a calculation mathematically rigorous and thus do not use this decomposition.

them [2]. Our results are manifestly in agreement with what observations have shown for many years.

In the solar wind, it has, relatively recently, become possible to probe beyond spectra and diagnose three-dimensional structure of local correlations [80, 81]. The physically motivated local basis is the direction of the “local mean” magnetic field (the correlation length along it is denoted  $\ell_{\parallel}$ ), the direction of the field’s perturbation  $\mathbf{b}$  at the scale of interest (the corresponding correlation length is  $\xi$ ) and the third direction, transverse to both (correlation length  $\lambda$ ). The idea is that, if turbulence has a tendency towards local alignment between the two Alfvénic fields [64, 65, 79, 82], it must turn out that statistically not only  $\lambda, \xi \ll \ell_{\parallel}$  (anisotropy) but also  $\lambda \ll \xi$  (alignment). In figure 6, we show representative contours of 3D correlation functions (“statistical eddy shapes”) calculated in this frame both for Alfvénic and compressive fluctuations. They are very similar to what is measured in the solar wind [80]: Alfvénic “statistical eddies” are “pancakes”, or “ribbons”, with  $\lambda \ll \xi \ll \ell_{\parallel}$ , while the compressive structures have a more tubular aspect.<sup>5</sup> Thus, it appears that simulated collisionless compressive fluctuations bear significant resemblance to the measured ones, in a more detailed way than just having the same spectra—a reassuring fact.

With the extraordinary velocity-space resolution afforded by the new MMS satellite, phase-space spectra have become measurable in space plasmas [10]. Thus, the prediction of steep Hermite spectra (figure 4) is a falsifiable one. More generally, considerations of phase-space turbulence can now be viewed as more than just theorizing about “under-the-hood” physics, for they deal with phenomena that are directly observable with available instruments.

**Implications for modelling techniques.** As we mentioned in the introduction, there is a thriving industry of effective fluid models of collisionless plasmas, of which the most sophisticated strand is the “Landau-fluid” closures [6, 7, 20, 21, 25–29]. Their underlying idea is to assume that Landau damping removes free energy from low to high Hermite moments as effectively in a nonlinear system as in a linear one. This might appear to be the exact opposite of the main conclusion of this work. However, Landau-fluid models have consistently been found to work better when more—but not necessarily many more—moments are kept compared to the standard fluid approximation. It might be argued that the art of crafting a good Landau-fluid model is precisely to do it in such a manner as to capture the effect of the echoes within a minimal set of Hermite moments while setting the boundary (closure) condition at the maximum retained  $m$  so as not to introduce or divert free-energy flows in a spurious way. With the echo effect and fluidization now explicitly part of one’s intellectual vocabulary, one might hope to revisit this task with renewed vigor, purpose and insight.

**An implication for astrophysical theory.** One cannot either adequately enumerate or, indeed, anticipate all of the instances across the vast canvas of plasma astrophysics where the nature of collisionless plasma turbulence may prove to be of interest.

<sup>5</sup>Quantitatively, for the Alfvénic fields, we see a scaling of the aspect ratio (very approximately) consistent with  $\lambda/\xi \propto \lambda^{1/4}$  [64, 65, 79], whereas for the compressive fluctuations,  $\lambda/\xi$  has a noticeably shallower scaling with  $\lambda$  (we do not measure these alignment scalings accurately at the resolution of our simulations). Thus, compressive fluctuations do appear to have a local 3D anisotropy and a tendency to form ribbons, but a weaker one than Alfvénic turbulence exhibits.

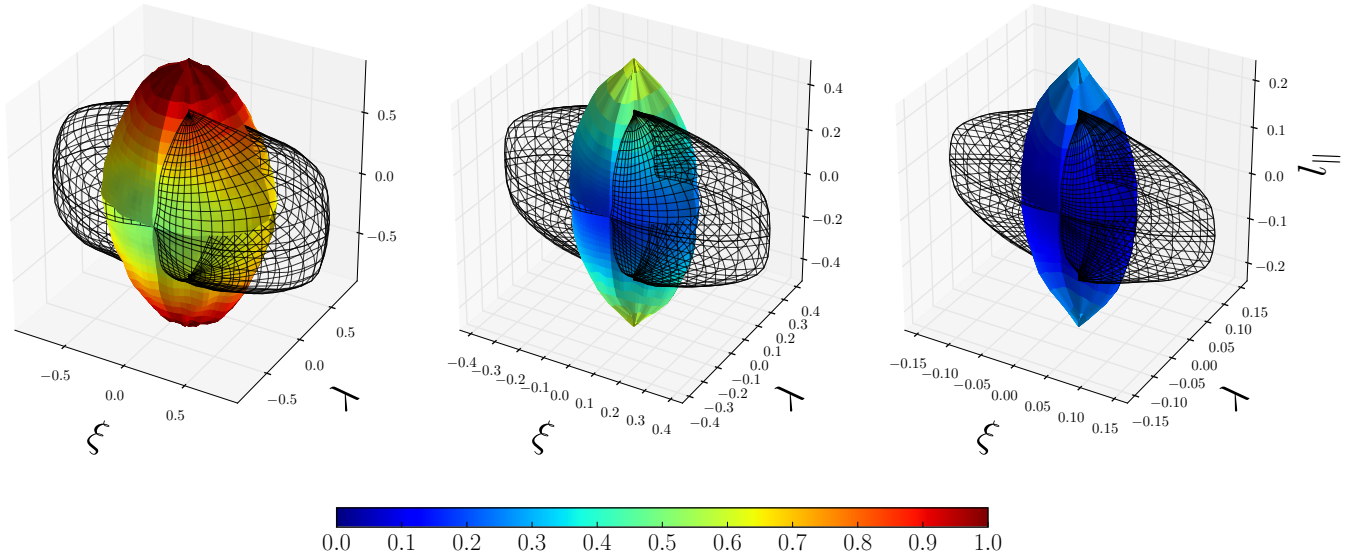


**Fig. 6.** Level sets for the correlation functions of the Alfvénic magnetic field  $\mathbf{b}$  (black netting) and perturbed field strength  $\delta B/B_0$  (color) corresponding to the perpendicular scales (from left to right)  $\lambda = 0.5, 0.16, 0.05$ . The two other coordinates are the distance  $\ell_{\parallel}$  along local mean field and the distance  $\xi$  along the perturbed field  $\mathbf{b}$ . Colors show distance from the center. Note that the parallel and perpendicular scales are measured in units of parallel and perpendicular box size, respectively ( $2\pi$  in each direction), which are also the forcing scales, but, in KRMHD, the box can be arbitrarily stretched in the parallel direction—so these level sets are in fact highly elongated with  $\ell_{\parallel} \gg \xi, \lambda$ . These correlation functions have been constructed following the method described in [79] and are to be compared, modulo the arbitrary elongation factor, with solar-wind measurements in [80].

We wish to highlight one problem that has a long history [83–85] and has recently seen a burst of activity (see [17] and references therein). It is a long-standing question in the theory of matter accretion onto black holes whether, and to what degree, plasma turbulence that is excited in the accretion disk by instabilities driven by the Keplerian shear and helps enable accretion by transporting angular momentum, can be thermalized preferentially on ions, rather than electrons, or vice versa. This has implications for the relative amounts of energy radiated out by electrons (and thus observed) vs. swallowed by the black hole as mass (ions) is sucked in, as well as for observational signatures of disks and their jets [86, 87]. Turbulent energy is split into Alfvénic and compressive cascades at MHD scales [2, 35]. Whereas at asymptotically low  $\beta_i$ , one can show that all of the compressive free energy must always thermalize into ions (this follows from the equations derived in [59]), how it is partitioned between ions and electrons at finite and high  $\beta_i$  is a nontrivial question decided by the dynamics at the ion Larmor scale [12, 13, 17, 88]—and so how much of it arrives to this scale without being dissipated on its way through the inertial range is important. Our findings indicate that, at least at  $\beta_i \sim 1$ , most of it does. Since the theory (or even a reliable modelling prescription) of energy partition in plasma turbulence is still to be developed, this is a useful factual constraint to have.

**Implications for general (plasma) physics.** The peregrinations and rearrangements of energy through a system’s phase space is a recurrent motif of theoretical physics. Turbulence theory is explicitly constructed to describe the energy’s thermalization routes, which bridge the usually vast separations between its injection and dissipation scales, producing rich, multiscale nonlinear structure in the process. In weakly collisional plasmas, these energy-transfer routes lie in a 6D phase space, with velocity-space refinement (phase mixing) of the particles’

distribution functions in general as effective as spatial mixing in accessing dissipation mechanisms [2, 56]. It is perhaps noteworthy that, in the case of inertial-range turbulence of a magnetized plasma, one of these forms of mixing turns out unambiguously to be the winner: spatial advection outperforms phase mixing and makes a collisionless plasma resemble a collisional fluid. Those who believe in the universality of nonlinear dynamics might be pleased by such an outcome. For plasma physicists, this is a sobering reminder that collisionless dissipation processes that make our subject so intellectually distinctive are not irreversible until they are consummated by collisional entropy production—and an intriguing demonstration that nonlinear effects can sometimes hinder them in favor of more “fluid-like” entropy-production mechanisms.

**ACKNOWLEDGMENTS.** We are grateful to T. Adkins, T. Antonson, A. Beresnyak, F. Califano, B. Chandran, S. Cowley, P. Dellar, G. Hammett, E. Highcock, Y. Kawazura, N. Loureiro, A. Mallet, J. Parker, C. Staines, and L. Stipani for many useful interactions on topics related to this project. This work was made possible thanks to the HPC resources of TGCC made available by GENCI (project A0010510117). W.D. and A.K. received support from US DoE (grants DE-FC02-04ER54784 and DE-FG02-93ER54197). The work of A.A.S. was supported in part by grants from UK STFC (ST/N000919/1) and EPSRC (EP/M022331/1). All authors gratefully acknowledge the hospitality of the Wolfgang Pauli Institute, Vienna, where some of this work was done.

- Schekochihin AA et al. (2008) Gyrokinetic turbulence: a nonlinear route to dissipation through phase space. *Plasma Phys. Control. Fusion* 50:124024.
- Schekochihin AA et al. (2009) Astrophysical gyrokinetics: kinetic and fluid turbulent cascades in magnetized weakly collisional plasmas. *Astrophys. J. Suppl.* 182:310.
- Kulsrud RM (1983) MHD description of plasma in *Handbook of Plasma Physics, Volume 1*, eds. Galeev AA, Sudan RN. (North-Holland, Amsterdam), p. 1.
- Kolmogorov AN (1941) Local structure of turbulence in incompressible viscous fluid at very large Reynolds numbers. *Dokl. Acad. Nauk SSSR* 30:299.
- Landau L (1946) On the vibration of the electronic plasma. *Zh. Eksp. Teor. Fiz.* 16:574.
- Hammett GW, Perkins FW (1990) Fluid moment models for Landau damping with application to the ion-temperature-gradient instability. *Phys. Rev. Lett.* 64:3019.
- Hammett GW, Dorland W, Perkins FW (1992) Fluid models of phase mixing, Landau damping, and nonlinear gyrokinetic dynamics. *Phys. Fluids B* 4:2052.

8. Kanekar A, Schekochihin AA, Dorland W, Loureiro NF (2015) Fluctuation-dissipation relations for a plasma-kinetic Langevin equation. *J. Plasma Phys.* 81:305810104.
9. Chen CHK (2016) Recent progress in astrophysical plasma turbulence from solar wind observations. *J. Plasma Phys.* 82:535820602.
10. Servidio S et al. (2017) Magnetospheric Multiscale (MMS) observation of plasma velocity-space cascade: Hermite representation and theory. *Phys. Rev. Lett.* 119:205101.
11. Howes GG et al. (2008) Kinetic simulations of magnetized turbulence in astrophysical plasmas. *Phys. Rev. Lett.* 100:065004.
12. Howes GG et al. (2011) Gyrokinetic simulations of solar wind turbulence from ion to electron scales. *Phys. Rev. Lett.* 107:035004.
13. Told D, Jenko F, TenBarge JM, Howes GG, Hammett GW (2015) Multiscale nature of the dissipation range in gyrokinetic simulations of Alfvénic turbulence. *Phys. Rev. Lett.* 115:025003.
14. Cerri SS, Kunz MW, Califano F (2018) Dual phase-space cascades in 3D hybrid-Vlasov-Maxwell turbulence. *Astrophys. J.* 856:L13.
15. Grošelj D, Mallet A, Loureiro NF, Jenko F (2018) Fully kinetic simulation of 3D kinetic Alfvén turbulence. *Phys. Rev. Lett.* 120:105101.
16. Franci L, Landi S, Verdini A, Matteini L, Hellinger P (2018) Solar wind turbulent cascade from MHD to sub-ion scales: large-size 3D hybrid particle-in-cell simulations. *Astrophys. J.* 853:26.
17. Kawazura Y, Barnes M, Schekochihin AA (2018) Thermal disequilibrium of ions and electrons by collisionless plasma turbulence. *E-print arXiv:1807.07702*
18. Weiland J (1992) Nonlinear effects in velocity space and drift wave transport in tokamaks. *Phys. Fluids B* 4:1388.
19. Hammett GW, Beer MA, Dorland W, Cowley SC, Smith SA (1993) Developments in the gyrofluid approach to tokamak turbulence simulations. *Plasma Phys. Control. Fusion* 35:973.
20. Dorland W, Hammett GW (1993) Gyrofluid turbulence models with kinetic effects. *Phys. Fluids B* 5:812.
21. Beer MA, Hammett GW (1996) Toroidal gyrofluid equations for simulations of tokamak turbulence. *Phys. Plasmas* 3:4046.
22. Hatch DR, Jenko F, Bratanov V, Bañón Navarro A (2014) Phase space scales of free energy dissipation in gradient-driven gyrokinetic turbulence. *J. Plasma Phys.* 80:531.
23. Schekochihin AA et al. (2016) Phase mixing versus nonlinear advection in drift-kinetic plasma turbulence. *J. Plasma Phys.* 82:905820212.
24. Parker JT, Highcock EG, Schekochihin AA, Dellar PJ (2016) Suppression of phase mixing in drift-kinetic plasma turbulence. *Phys. Plasmas* 23:070703.
25. Snyder PB, Hammett GW, Dorland W (1997) Landau fluid models of collisionless magnetohydrodynamics. *Phys. Plasmas* 4:3974.
26. Snyder PB, Hammett GW (2001) A Landau fluid model for electromagnetic plasma microturbulence. *Phys. Plasmas* 8:3199.
27. Passot T, Sulem PL (2004) A Landau fluid model for dispersive magnetohydrodynamics. *Phys. Plasmas* 11:5173.
28. Sulem PL, Passot T (2015) Landau fluid closures with nonlinear large-scale finite Larmor radius corrections for collisionless plasmas. *J. Plasma Phys.* 81:325810103.
29. Tassi E, Sulem PL, Passot T (2016) Reduced models accounting for parallel magnetic perturbations: gyrofluid and finite Larmor radius-Landau fluid approaches. *J. Plasma Phys.* 82:705820601.
30. Howes GG et al. (2008) A model of turbulence in magnetized plasmas: implications for the dissipation range in the solar wind. *J. Geophys. Res.* 113:A05103.
31. Podesta JJ, Borovsky JE, Gary SP (2010) A kinetic Alfvén wave cascade subject to collisionless damping cannot reach electron scales in the solar wind at 1 AU. *Astrophys. J.* 712:685.
32. Howes GG (2010) A prescription for the turbulent heating of astrophysical plasmas. *Mon. Not. R. Astron. Soc.* 409:L104.
33. Passot T, Sulem PL (2015) A model for the non-universal power law of the solar wind sub-ion-scale magnetic spectrum. *Astrophys. J.* 812:L37.
34. Kunz MW, Abel IG, Klein KG, Schekochihin AA (2018) Astrophysical gyrokinetics: turbulence in pressure-anisotropic plasmas at ion scales and beyond. *J. Plasma Phys.* 84:715840201.
35. Lithwick Y, Goldreich P (2001) Compressible magnetohydrodynamic turbulence in interstellar plasmas. *Astrophys. J.* 562:279.
36. Celnikier LM, Harvey CC, Jegou R, Moricet P, Kemp M (1983) A determination of the electron density fluctuation spectrum in the solar wind, using the ISEE propagation experiment. *Astron. Astrophys.* 126:293.
37. Celnikier LM, Muschietti L, Goldman MV (1987) Aspects of interplanetary plasma turbulence. *Astron. Astrophys.* 181:138.
38. Marsch E, Tu CY (1990) Spectral and spatial evolution of compressible turbulence in the inner solar wind. *J. Geophys. Res.* 95:11945.
39. Bershadskii A, Sreenivasan KR (2004) Intermittency and the passive nature of the magnitude of the magnetic field. *Phys. Rev. Lett.* 93:064501.
40. Hnat B, Chapman SC, Rowlands G (2005) Compressibility in solar wind plasma turbulence. *Phys. Rev. Lett.* 94:204502.
41. Kellogg PJ, Horbury TS (2005) Rapid density fluctuations in the solar wind. *Ann. Geophys.* 23:3765.
42. Chen CHK, Bale SD, Salem C, Mozer FS (2011) Frame dependence of the electric field spectrum of solar wind turbulence. *Astrophys. J.* 737:L41.
43. Barnes A (1966) Collisionless damping of hydromagnetic waves. *Phys. Fluids* 9:1483.
44. Goldreich P, Sridhar S (1995) Toward a theory of interstellar turbulence. 2: Strong Alfvénic turbulence. *Astrophys. J.* 438:763.
45. Goldreich P, Sridhar S (1997) Magnetohydrodynamic turbulence revisited. *Astrophys. J.* 485:680.
46. Verscharen D, Chen CHK, Wicks RT (2017) On kinetic slow modes, fluid slow modes, and pressure-balanced structures in the solar wind. *Astrophys. J.* 840:106.
47. Gould RW, O'Neil TM, Malmberg JH (1967) Plasma wave echo. *Phys. Rev. Lett.* 19:219.
48. Malmberg JH, Wharton CB, Gould RW, O'Neil TM (1968) Plasma wave echo experiment. *Phys. Rev. Lett.* 20:95.
49. Frieman EA, Chen L (1982) Nonlinear gyrokinetic equations for low-frequency electromagnetic waves in general plasma equilibria. *Phys. Fluids* 25:502.
50. Howes GG et al. (2006) Astrophysical gyrokinetics: basic equations and linear theory. *Astrophys. J.* 651:590.
51. Kunz MW, Schekochihin AA, Chen CHK, Abel IG, Cowley SC (2015) Inertial-range kinetic turbulence in pressure-anisotropic astrophysical plasmas. *J. Plasma Phys.* 81:325810501.
52. Kadomtsev BB, Pogutse OP (1974) Nonlinear helical perturbations of a plasma in the tokamak. *Soviet Phys. JETP* 38:283.
53. Strauss HR (1976) Nonlinear, three-dimensional magnetohydrodynamics of noncircular tokamaks. *Phys. Fluids* 19:134.
54. Elsasser WM (1950) The hydromagnetic equations. *Phys. Rev.* 79:183.
55. Eyink GL (2015) Turbulent general magnetic reconnection. *Astrophys. J.* 807:137.
56. Eyink GL (2018) Cascades and dissipative anomalies in nearly collisionless plasma turbulence. *E-print arXiv:1803.03691*
57. Boozer AH (2018) Why fast magnetic reconnection is so prevalent. *J. Plasma Phys.* 84:715840102.
58. Bratanov V, Jenko F, Hatch DR, Wilczek M (2013) Nonuniversal power-law spectra in turbulent systems. *Phys. Rev. Lett.* 111:075001.
59. Zocco A, Schekochihin AA (2011) Reduced fluid-kinetic equations for low-frequency dynamics, magnetic reconnection, and electron heating in low-beta plasmas. *Phys. Plasmas* 18:102309.
60. Kanekar AV (2015) Phase mixing in turbulent magnetized plasmas. *Ph. D. Thesis.* University of Maryland, College Park (URL: <http://drum.lib.umd.edu/handle/1903/16418>).
61. Adkins T, Schekochihin AA (2018) A solvable model of Vlasov-kinetic plasma turbulence in Fourier-Hermite phase space. *J. Plasma Phys.* 84:905840107.
62. Patterson, Jr. GS, Orszag SA (1971) Spectral calculations of isotropic turbulence: efficient removal of aliasing interactions. *Phys. Fluids* 14:2538.
63. Teaca B, Lalescu CC, Knaepen B, Carati D (2011) Controlling the local invariant fluxes for MHD turbulence using TURBO spectral solver. *E-print arXiv:1108.2640*
64. Boldyrev S (2006) Spectrum of magnetohydrodynamic turbulence. *Phys. Rev. Lett.* 96:115002.
65. Mallet A, Schekochihin AA (2017) A statistical model of three-dimensional anisotropy and intermittency in strong Alfvénic turbulence. *Mon. Not. R. Astron. Soc.* 466:3918.
66. Maron J, Goldreich P (2001) Simulations of incompressible magnetohydrodynamic turbulence. *Astrophys. J.* 554:1175.
67. Chen CHK, Mallet A, Yousef TA, Schekochihin AA, Horbury TS (2011) Anisotropy of Alfvénic turbulence in the solar wind and numerical simulations. *Mon. Not. R. Astron. Soc.* 415:3219.
68. Perez JC, Mason J, Boldyrev S, Cattaneo F (2012) On the energy spectrum of strong magnetohydrodynamic turbulence. *Phys. Rev. X* 2:041005.
69. Obukhov AM (1949). *Izv. Akad. Nauk SSSR Ser. Geogr. Geofiz.* 13:58.
70. Corrsin S (1951) On the spectrum of isotropic temperature fluctuations in an isotropic turbulence. *J. Applied. Phys.* 22:469.
71. Mallet A, Schekochihin AA, Chandran BDG (2015) Refined critical balance in strong Alfvénic turbulence. *Mon. Not. R. Astron. Soc.* 449:L77.
72. Beresnyak A (2015) On the parallel spectrum in magnetohydrodynamic turbulence. *Astrophys. J.* 801:L9.
73. Horbury TS, Forman M, Oughton S (2008) Anisotropic scaling of magnetohydrodynamic turbulence. *Phys. Rev. Lett.* 101:175005.
74. Podesta JJ (2009) Dependence of solar-wind power spectra on the direction of the local mean magnetic field. *Astrophys. J.* 698:986.
75. Wicks RT, Horbury TS, Chen CHK, Schekochihin AA (2010) Power and spectral index anisotropy of the entire inertial range of turbulence in the fast solar wind. *Mon. Not. R. Astron. Soc.* 407:L31.
76. Cho J, Vishniac ET (2000) The anisotropy of magnetohydrodynamic Alfvénic turbulence. *Astrophys. J.* 539:273–282.
77. Pezzi O et al. (2018) Velocity-space cascade in magnetized plasmas: numerical simulations. *Phys. Plasmas* 25:060704.
78. Verma MK (2004) Statistical theory of magnetohydrodynamic turbulence: recent results. *Phys. Rep.* 401:229.
79. Mallet A et al. (2016) Measures of three-dimensional anisotropy and intermittency in strong Alfvénic turbulence. *Mon. Not. R. Astron. Soc.* 459:2130.
80. Chen CHK et al. (2012) Three-dimensional structure of solar wind turbulence. *Astrophys. J.* 758:120.
81. Verdini A, Grappin R, Alexandrova O, Lion S (2018) 3D anisotropy of solar wind turbulence: tubes or ribbons? *Astrophys. J.* 853:85.
82. Chandran BDG, Schekochihin AA, Mallet A (2015) Intermittency and alignment in strong RMHD turbulence. *Astrophys. J.* 807:39.
83. Rees MJ, Begelman MC, Blandford RD, Phinney ES (1982) Ion-supported tori and the origin of radio jets. *Nature* 295:17.
84. Narayan R, Yi I (1995) Advection-dominated accretion: underfed black holes and neutron stars. *Astrophys. J.* 452:710.
85. Quataert E, Gruzinov A (1999) Turbulence and particle heating in advection-dominated accretion flows. *Astrophys. J.* 520:248.
86. Ressler SM, Tchekhovskoy A, Quataert E, Gammie CF (2017) The disc-jet symbiosis emerges: modelling the emission of Sagittarius A\* with electron thermodynamics. *Mon. Not. R. Astron. Soc.* 467:3604.
87. Chael A, Rowan M, Narayan R, Johnson M, Sironi L (2018) The role of electron heating physics in images and variability of the Galactic Centre black hole Sagittarius A\*. *Mon. Not. R. Astron. Soc.* 478:5209.
88. Parashar TN, Matthaeus WH, Shay MA (2018) Dependence of kinetic plasma turbulence on plasma beta. *E-print arXiv:1807.11371*